A family of high-flow Roots blower profiles based on non-circular gears and the coin rotation paradox

Robert W. Horst[1,2]

[1]*Dept. of Electrical and Computer Engineering, University of Illinois at Urbana-Champaign, USA*
[2]*Horst Tech, LLC, Bellevue, Washington, USA*

Correspondence should be addressed to Robert Horst, bhorst@illinois.edu

Abstract

Roots blowers are positive displacement pumps that trap the air in pockets of counter-rotating rotors. This paper describes and analyzes a new family of high-flow Roots blower profiles. Models and tests show that the new profiles may have flow rates greater than four times the flow rate of those based on epicycloid/hypocycloid arcs. The profiles can be used to build either straight-lobe or helical rotors. For a given airflow requirement, the new profiles allow for reduced RPM, lower acoustic noise, lower power and lower weight. These benefits may open up new applications for Roots blowers in consumer applications. Simplified equations for the profiles of a circle rolling around a noncircular gear are derived using the lessons from the coin rotation paradox. The equations take advantage of previous work in noncircular gear theory but advance that theory to produce an equation that produces a range of identical noncircular gears with any number of lobes. Clearances between the rotors are adjusted by offsetting the profiles. The resulting profiles are more eccentric and have higher flow than traditional Roots profiles. Estimates and measurements of the flow rates show that the small amount of carryover (reverse flow) is more than overcome by the greater flow rates of the new profiles. Multiple variations of the profiles are illustrated by figures showing the meshing of rotors at different angles. Publicly available MATLAB® code that can be used to graph and analyze different profiles and to export data to mechanical CAD programs for fabricating the rotors.

Keywords *Roots blower; noncircular gear; rotor profile; rotary lobe pump; helical rotor*

1. Introduction

Roots blowers, also known as rotary lobe blowers, are positive displacement pumps that move air by trapping the air in pockets of counter-rotating rotors. The pockets are formed by the space between the rotors and the casing. The original Roots blower used two-lobed rotors, but other rotor profiles with three or more lobes are now common. Roots blowers are used to move or compress air or gasses in a wide variety of industries but have seen little application in consumer blowers or in electronics cooling. This paper offers an improvement in the flow rate of Roots blowers that may make them more suitable for those uses.

Figure 1 shows an example of a 3-lobed rotor with air entering the suction (input) port, flowing around the outside of both rotors, and exiting from the discharge (output) port. The original Roots

blower designs, and many subsequent improvements, have restricted the allowable profiles to keep the gaps between them at the lowest possible values given the manufacturing tolerances. This paper instead creates a family of profiles that provide much greater net airflow while allowing for greater gaps between the rotors and also tolerating looser manufacturing tolerances.

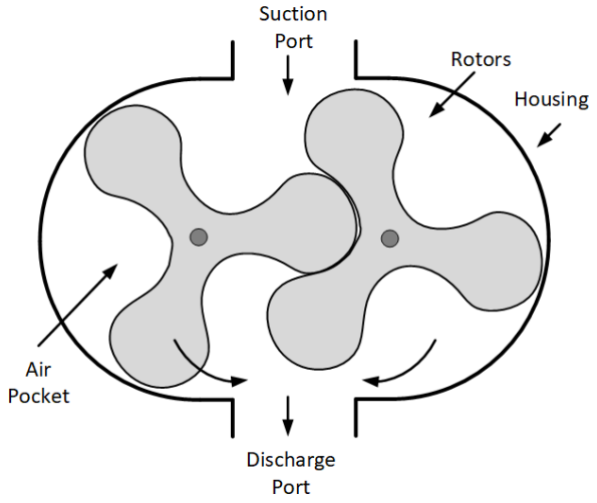

Figure 1. 3-lobe Roots blower cross section

Nomenclature

N	Number of lobes of noncircular gear
α	Semi-major axis of noncircular gear in mm
β	Semi-minor axis of noncircular gear in mm
ε	Eccentricity of noncircular gear = $\sqrt{1-\left(\frac{\beta^2}{\alpha^2}\right)}$ For a circle, ε = 0.
θ	Angle around noncircular gear or rotor (0-2π)
ss	Shaft spacing in mm
$\rho_1(\theta)$	Polar coordinate radius of the first gear at angle θ
$\rho_2(\theta)$	Polar coordinate radius of the second gear at angle -θ to mesh with first gear
$\Delta_\rho(\theta)$	Radius correction in mm to first and second gears to make them mesh and identical
$\rho_3(\theta)$	Corrected radius of the first gear
$\rho_4(\theta)$	Corrected radius of the second gear
r_c	Radius of the rolling circle in mm
P_x, P_y	Rectangular coordinates of the rotor profile in mm
ϕ	Rotation angle of a fixed point on the circle as it rotates around the noncircular gear
offset	Distance in mm subtracted from the rotor radius at every angle to prevent interference
gap	Space between rotors in mm. The gap is computed numerically for each rotation angle.
rmax, rmin,	Maximum and minimum radius in mm from shaft center to the outer edge of rotor
wmin	Minimum width of the rotor in mm.
λ_r, λ_w	Rotor lobe aspect ratios. λ_r = *rmin*/*rmax* , λ_w = *wmin*/*rmax*.
area efficiency	% of air area in rotation path = (swept_area - rotor_area)/swept_area

2. Prior work in Roots blower profiles

Roots blower profiles have undergone a series of modifications and improvements since the concepts of the Roots Blower was invented and patented by the Roots brothers [1]. In 1873, the profile was modified by Palmer and Knox to form the addendum and dedendum from an epicycloid and hypocycloid (EH), respectively [2]. This EH profile is formed by a point on the circumference of a rolling circle that rolls around the outside of the pitch circle to generate the epicycloid, and rolls around the inside of the pitch circle to generate the hypocycloid. The EH profile is often the basis for comparison to newer profiles. The 2018 paper by Wu and Tran presents the equations for EH profiles along with a CIC profile. The CIC rotor profile is comprised of a circular arc, an involute curve and a conjugated circular arc [3]. The CIC profile was also analyzed in the 1980 paper by Ucer and Celik [4].

Zauo, in a 2023 paper, proposes a novel Roots profile that consists of six curves and a sharp point [5]. These profiles involve increasing complexity. The Zauo paper has four reference coordinate systems and two full pages of parametric equations. While this profile is an improvement over some prior profiles, the math complexity makes it a daunting task for an engineer to implement.

Several papers have suggested generating Roots profiles by rolling a circle or ellipse outside and inside a pitch path. With a circular roller and circular pitch path, this method generates the standard epicycloid-hypocycloid profiles introduced in 1873. Tien proposed a Roots profile based on rolling a circle around an ellipse [6].

The Roots profiles in this paper are based on rolling a circle around identical noncircular gear pitch profiles. A theory for generating these noncircular pitch curves was presented in 1998 by Tong [7]. The pitch curves can also be generated based on the noncircular gears presented by Litvin and Bair [8,9]. These papers present noncircular gears based on a driven gear, with the conjugate gear profile determined by the spacing and phase of the driven gear. The equation for an N-lobe driven gear is given by:

$$\rho_1(\theta) = \frac{a(1-\varepsilon)}{1+\varepsilon(\cos(N * \theta))} \tag{1}$$

Where ρ is the radius at each angle θ, α is the semi-major axis distance, ε is the eccentricity and N is the number of lobes. The conjugate noncircular gear equation is simply:

$$\rho_2(\theta) = ss - \rho\_1(\theta) \tag{2}$$

where ss is the shaft spacing.

While Eq 1 and Eq 2 can be used for noncircular gearing, the two gears are not identical. Generating Roots profiles requires the noncircular gears to have identical pitch profiles. If Equation 1 is used for both gears, but with the second gear rotated by 90°, they mesh at the 90° rotation intervals, but do not quite mesh in between. A correction can be made, with half the correction made to each gear to make identical gears that mesh at all rotation angles. Then the equations for the radius of the identical N-lobe noncircular gears at angle θ are:

$$\begin{cases} \rho_3(\theta) = \dfrac{a(1-\varepsilon^2)}{1+\varepsilon(\cos(N*\theta))} + \dfrac{\Delta_\rho(\theta)}{2} \\ \rho_4(\theta) = \dfrac{a(1-\varepsilon^2)}{1+\varepsilon\left(\cos\left(\frac{\pi}{N}+N*\theta\right)\right)} + \dfrac{\Delta_\rho(\theta)}{2} \\ \Delta_\rho(\theta) = ss - \dfrac{a(1-\varepsilon^2)}{1+\varepsilon(\cos(N*\theta))} - \dfrac{a(1-\varepsilon^2)}{1+\varepsilon\left(\cos\left(\frac{\pi}{N}+N*\theta\right)\right)} \end{cases} \quad (3)$$

Figure 2 shows three-lobe noncircular gears with and without the correction to make them mesh at all pitch angles.

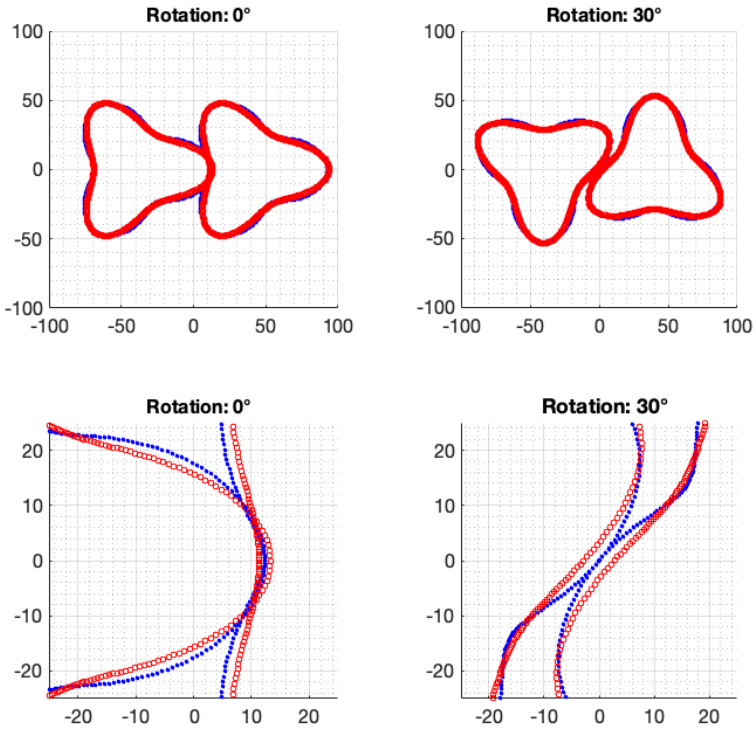

Figure 2. Full and closeup profiles of three-lobe noncircular gears with ε = 0.3 at two different rotation angles. The red circles show identical uncorrected profiles from Equation 1 and the blue points show the corrected profiles from Equation 3. X and Y axis units are in mm for rotors with shaft spacing of 80.4 mm, but the shapes can be scaled to any dimension.

In Figure 2, at 0º rotation there is interference between the uncorrected gear profiles and at 30º, there is a gap between the uncorrected gear profiles. The corrected profiles have no interference or gaps at any rotation angle.

This approach is a contribution to noncircular gearing that extends the work previously presented in [7-9]. The simple corrections from Equation 3 offer a way to make a class of identical multi-lobe noncircular gears that mesh perfectly at all rotation angles.

3. Profiles based on rolling a circle around noncircular gears

Tien et. al. proposed a Roots profile based on rolling a circle around an ellipse, but the paper does not extend the idea to more than two lobes and does not discuss corrections to make center-axis ellipses mesh at all angles [11].

The Roots blower profiles in this paper are based on rolling a circle around a noncircular gear profile. Any type of center-axis, identical gear could be used, including those proposed by Tong [10] but this paper presents only the noncircular gears based on Equation 3 above. The radius of the rolling circle, r_c, is determined by the number of lobes and the circumference of the noncircular gear.

$$r_c = \frac{\int_0^{2\pi} \rho(\theta) d\theta}{4\pi N} \tag{4}$$

The circumference of the noncircular gear is determined by converting the points to polar notation and numerically integrating the radius of the gear from 0 to 2π. The denominator is set to allow the circle radius to fully rotate once for each addendum and once for each dedendum. With 2 lobes, the rolling distance around the noncircular gear is $8\pi r_c$ and with 3 lobes, the distance is $12\pi r_c$.

The lobes are formed by rolling on the outside of the gear for the addendum and rolling on the inside of the gears for the dedendum. This allows the math to be greatly simplified relative to other papers that derive complex parametric equations based on translation between different reference frames and determining a constant rate of curvature at transition points between addendum and dedendum.

The rolling of a circle around another shape is a form of a problem known as the coin rotation paradox [13]. When rolling a coin around one with three times the diameter, to get back to the original position, it rotates four times, not three times. This can be understood by rolling the coin along a straight belt with length three times the circumference of the small coin. When that belt is then wrapped around the large coin, it rotates one more time. Another way to understand this paradox is to visualize the rotation of one coin with radius r_1, around a second coin of radius r_2. With identical coins ($r_1 = r_2$), the second coin must make two full rotations before returning to its initial position. Generalizing to coins of any radius, the number of rotations $n = r_1/r_2 + 1$. The same relationship holds with shapes other than circular, but the radii may change at each rotation angle.

In the case of a circle rotating around a noncircular gear, the circle rotates once on the outside of the gear for each addendum and once on the inside for each dedendum. The position of a point on the circle is the position of the center of the circle plus the rotation of the circle around its center. For the addendum of a 2-lobe rotor, the circle rotates 4 + 1 = 5 degrees for every one degree of change around the gear perimeter. For the dedendum, rolling on the inside, it rotates 4 - 1 = 3 degrees for every one degree of change around the gear perimeter. For a 3-lobe rotor, it rotates 7 times for the addendum and 5 times for the dedendum. The equations for an N-lobe rotor are simply:

Addendum

$$\begin{cases} \phi = \theta(2N+1) \\ P_x = (\sigma_3 + r_c)\cos\theta + r_c\cos\phi \\ P_y = (\sigma_3 + r_c)\sin\theta + r_c\sin\phi \end{cases} \tag{5}$$

Dedendum

$$\begin{cases} \phi = \theta(2N-1) \\ P_x = (\sigma_3 - r_c)\cos\theta - r_c\cos\phi \\ P_y = (\sigma_3 - r_c)\sin\theta - r_c\sin\phi \end{cases} \quad (6)$$

where θ is the angle from the X axis to the point (P_x and P_y) of the rotor, r_c is the radius of the rolling circle, and ϕ is the rotation angle of the circle. For the addendum, the center of the circle is the sum of the radius of the gear and the circle, while for the dedendum, the center of the circle is the gear radius minus the circle radius. The circle rotation direction is positive for the addendum and negative for the dedendum.

3.1. Interference and gaps

The rotor profiles generated by the rolling circle mesh perfectly if the noncircular gear is convex, such as when $\varepsilon = 0$ (with the gear shape a circle). However, at larger values of ε, the noncircular gear is partially concave, and if the radius of curvature of the concave portion is less than that of the circle, the resulting gear shapes interfere with each other at some rotation angles.

One way to solve the interference problem is simply to avoid the problem by restricting the solution set to less eccentric designs that avoid the interferences. This paper takes a different approach and allows more eccentric rotor shapes by offsetting the profiles to reduce the rotor radius at all angles to at least the point where the interference is avoided. This reduction introduces undercutting and carryover volume, which are normally avoided in Roots profile design. (Carryover is the term that describes air that is trapped and returned to the input or recirculated, instead of being delivered to the discharge port.) However, the approach taken here more than makes up for the carryover volume by increased airflow due to the improved area efficiency.

3.2. Offsets

To create the offset profile, at each point, the normal angle is derived as 90° from the tangent angle, then the radius at that angle is reduced by the *offset* value. Alternatively, the new profile can be derived using the MATLAB *offsetCurve* function, or by using a 3D CAD tool such as the Autodesk Fusion *Offset* feature. To determine when *offset* is large enough to avoid all interferences, a simple brute-force approach has been used to measure the distance between all points of both profiles at a large number of rotation angles. For Figures 4-6 and tables 1-2, 360 rotation angles are used with 1001 points for the rotor profiles. The MATLAB code to determine minimum gaps for a given offset was first written as a triple-nested loop, but each offset value took several minutes to analyze. By vectorizing the MATLAB code, this time was reduced to a few seconds. The vector code was used to find profiles with 0.1, 2 and 7 mm minimum gaps. The average gaps were also determined for the airflow calculations.

Figure 3 shows the construction of 2-lobe and 3-lobe rotors with 0.1 mm minimum gaps. The solid lines are the noncircular gear shapes used to generate the rotor profiles.

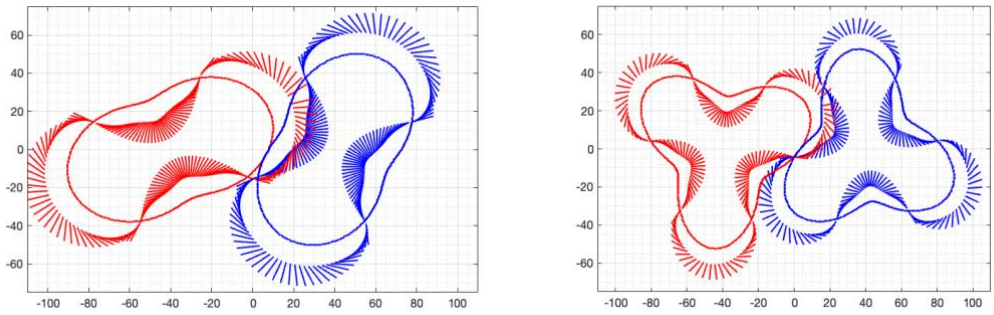

Figure 3. Derivation of Roots profiles from rolling a circle outside and inside a 2-lobe or 3-lobe noncircular gear with ε = 0.3 and 180 points. Straight lines connect the center of the rolling circle to the point on the circle defining the profile. X and Y axis units are in mm for rotors with shaft spacing of 80.4 mm

Figure 4 illustrates Roots profiles after applying the offsets. The illustrated shapes include offsets that can be adjusted to avoid interference between the rotors. Before the offset is applied, the rotors would interfere with each other. The offset is adjusted until the minimum rotor-rotor gap is the desired gap, based on the manufacturing tolerances. This figure also illustrates the large difference in air pocket volume for designs with higher eccentricity.

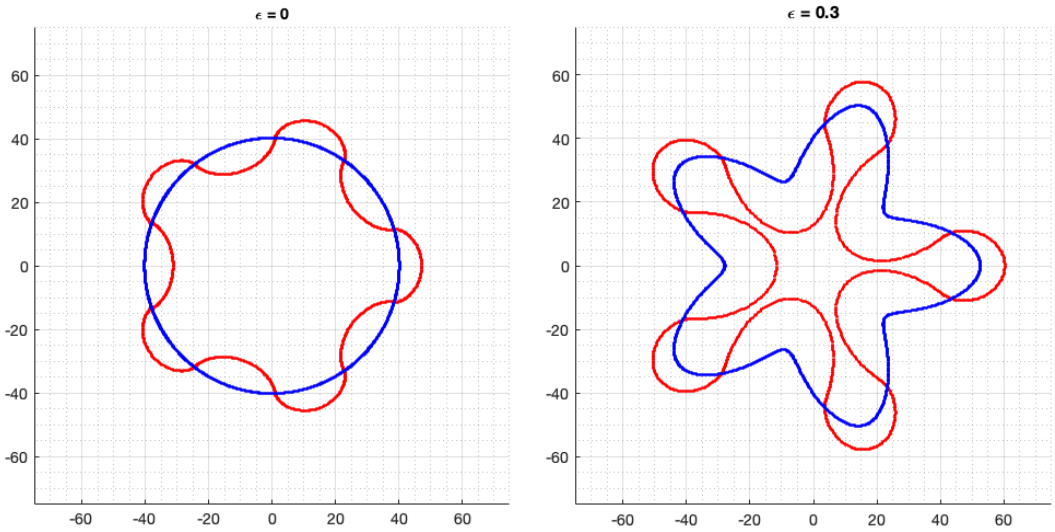

Figure 4. Five lobe rotors showing the noncircular gear in blue and the final offset rotor shape in red. The left rotor is the standard epicycloid-hypocycloid shape based on rolling a circle (ε = 0) around a larger circle. The right rotor is based on noncircular gears with ε = 0.3 and has a calculated flow rate 3.9 times greater. X and Y axis units are in mm for rotors with shaft spacing of 80.4 mm

Figure 5 shows graphs of the minimum inter-rotor gap (in mm) vs. rotation angle (in degrees) for several different rotor shapes. When the "noncircular" gear is in fact circular, with ε = 0, the minimum gap is equal to twice the offset and does not vary with rotation angle. With ε > 0, there are periodic peaks in the minimum gap, indicating the condition known in gear design as *undercutting*. At these angles, a pocket is formed in the gap between the rotors, and the rotor exhibits *carryover*, a reverse flow where some air is returned to the input instead of being delivered to the output. The effect of this carryover volume is analyzed in the section on airflow estimates.

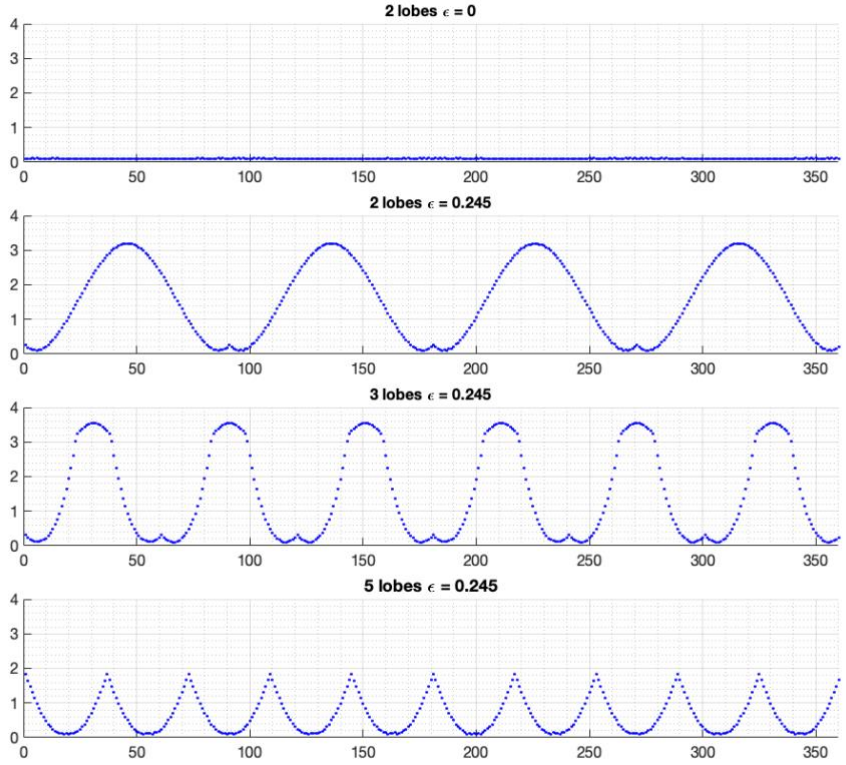

Figure 5. Minimum gap vs rotation angle for profiles with 2, 3 and 5 lobes. X axis is in degrees, Y axis is in mm. Offsets are set to make the minimum gaps 0.1 mm (See Table 2).

4. Rotor profiles

Figure 6 shows rotor profiles for 2-5 lobes for a range of ε values. This figure also shows the noncircular gears used to derive each profile. Note that the air volume increases as ε increases, but at some point, a limit is eventually reached. For 2-lobe rotors, the minimum rotor radius decreases sharply and eventually reaches a point where it is too small for the required shaft and bearings to support the rotor. With a greater number of lobes, another constraint is encountered when the minimum lobe widths become too thin to maintain their shape. An engineer can select among the different profiles in the family to find one with the highest airflow that meets the constraints for the required minimum rotor radius and minimum lobe width for the intended application.

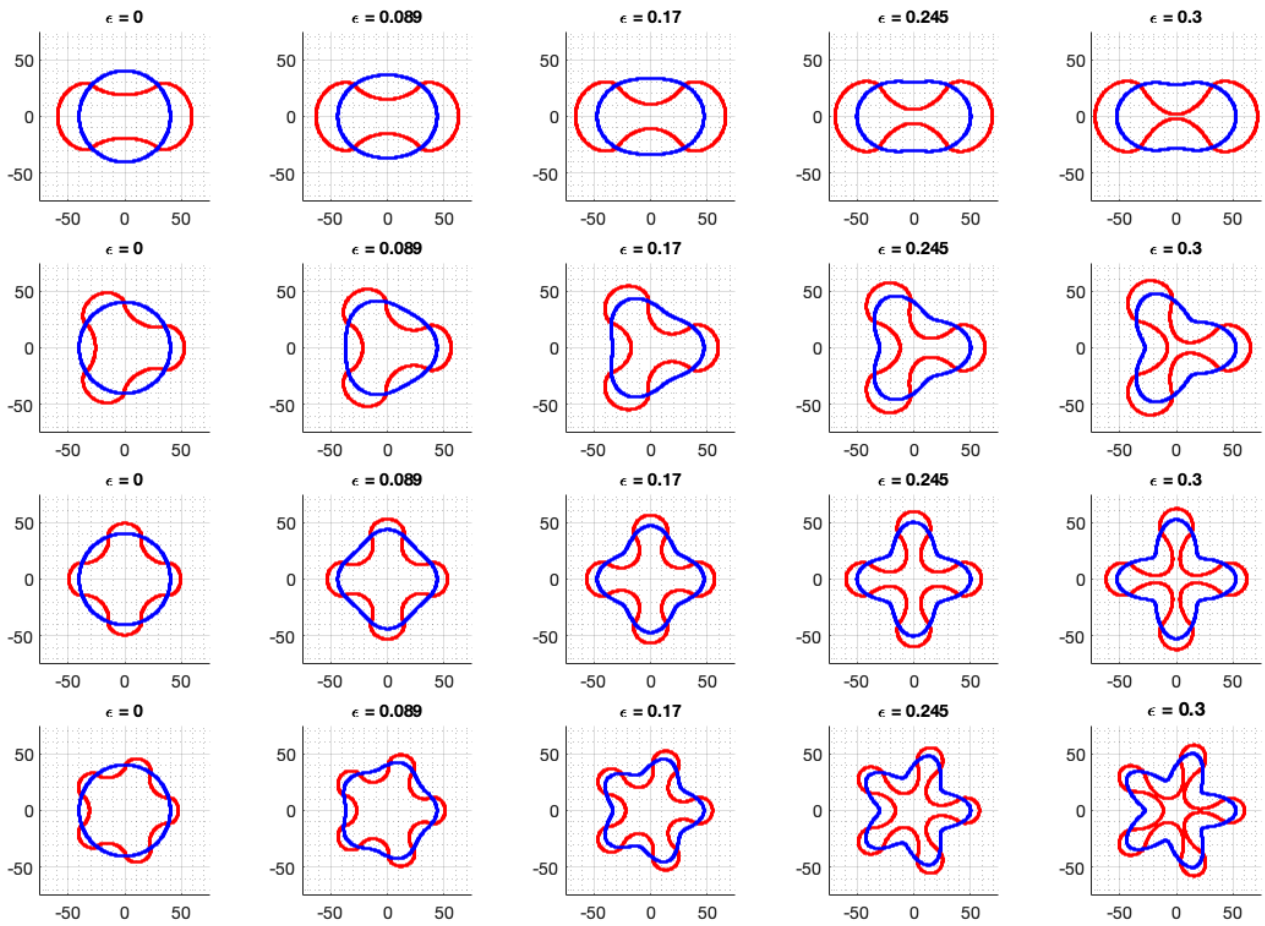

Figure 6. Roots rotor profiles with 2-5 lobes. Blue lines show the noncircular gear profiles, and red lines show the resulting rotor profiles from rolling a circle inside and outside the gears. X and Y axis units are in mm for rotors with shaft spacing of 80.4 mm

4.1. Air flow estimates

Each lobe of a rotor moves a pocket of air from the suction port to the discharge port. The pocket is formed from the volume of air trapped between the rotor and the housing. In one rotation, all lobes of both rotors deliver the air in their trapped pockets to the discharge port. For one rotation, the volume of air can be computed from the area of the minimum circle around the rotor minus the area of the rotor itself. The ratio of this air volume to the circle area is known as the *area utilization efficiency*, *area efficiency, or area utilization ratio*. The volume of air moved per revolution of each rotor is the non-rotor area within the circle multiplied by the rotor height. The volume is multiplied by the motor RPM to calculate the maximum output flow per rotor, then doubled to get the maximum output of the blower.

4.2. Gaps

Gaps between the rotors, as shown in Figure 5, reduce the flow because of the imperfect mismatch of the rotor profiles. Additional inter-rotor gaps may also be added into the offset to allow

for manufacturing tolerances. The volume of air in the rotor gaps is recirculated or returned to the discharge port, reducing the net flow. The following tables use a version of the technique suggested by Ucer [14] to estimate the net flow. Air trapped in the gaps is treated like a separate port that delivers reverse airflow from the discharge port to the suction port. This leakage flow is estimated by computing the gap area as the average gap during a full rotation times the average radius at which the gap volume is delivered back to the input port. The average radius is just the average of the minimum and maximum rotor radii. This area is multiplied by the rotor height to get the volume and then multiplied by the RPM to get the airflow loss. It is assumed that the entire gap air volume is delivered back to the suction port, reducing the flow by that amount. The backflow analysis makes the same assumptions as Ucer:

> "The modelling is done by assuming that the working fluid is perfect gas, all processes are adiabatic. Wave action is not considered in the inlet tract, outlet port and trapped pocket. Flow at the boundaries of the blower is assumed to be quasi-steady. Mixing processes are considered to proceed instantaneously to homogeneous equilibrium. It is also assumed that the flow to the throat of a constriction is isentropic. This assumption is used in calculating the backflow from the outlet port to the trapped pocket." Ucer [4]

4.3. Rotor comparisons

Table 1 shows the results of an airflow model written in MATLAB. The inputs and derived values correspond to the profiles illustrated in Figure 6. The three input parameters that generate rotor profiles are the three left columns (*lobes*, *gear* ε, and *offset*). Other fixed input values (shaft spacing, rotor height, and motor RPM) are used for all calculations. The other columns show the airflow loss, net airflow, and other derived parameters.

The chamber volume of each rotor is the product of the rotor height and the swept area of the lobes; swept area is the area of a circle with radius equal to the maximum length of each rotor. Area efficiency is computed by dividing the total rotor area by the swept area.

The derivation of airflow is based on a simplified model that does not take into account the leakage or boundary conditions. The model is primarily presented to contrast the proposed new profiles with the standard epicycloid-hypocycloid profiles ($\varepsilon = 0$). More detailed models or finite-element analysis could give more accurate absolute results but would be unlikely to have much effect on the ratio of airflow improvements from different profiles. The experimental evidence in Section 4.6 supports this assumption.

In the analysis, all thermodynamic properties are evaluated at laboratory ambient conditions corresponding to the experiments (air temperature approximately 22 °C, atmospheric pressure ≈1 atm). The working fluid is modeled as an ideal gas under these conditions, with properties assumed constant over this temperature range.

Table 1. Airflow model with rotor height 100 mm, shaft spacing 80.4 mm, and rotor-to-housing gap of 2 mm. The left three columns are the input values and the other columns are derived by the model. *Offset* inputs are set to values that make the minimum rotor-rotor gaps close to 2 mm. Offsets, gaps, lobes and housing dimensions are all in mm. Airflow is the total flow for the Roots blower while running at 1000 RPM.

Lobes	Gear ε	Offset	Gaps min/avg	Lobes *rmax* x *rmin* x *wmin*	Housing diam	λ_r / λ_w	Area Efficiency	Airflow (m^3/min) loss	net	ratio
2	0	1	2.00 - 2.00	59.3 x 19.1 x 55.4	122.6	0.32/0.93	0.51	0.05	1.1	1
2	0.089	1.17	2.00 - 2.16	62.8 x 15.1 x 30.3	129.7	0.24/0.48	0.55	0.05	1.3	1.2
2	0.17	1.7	2.00 - 2.59	65.9 x 10.5 x 21.5	135.9	0.16/0.33	0.59	0.06	1.6	1.4
2	0.245	2.54	2.00 - 3.44	68.7 x 5.3 x 11.9	141.4	0.08/0.17	0.63	0.08	1.8	1.6
2	0.3	3.4	2.02 - 4.50	70.7 x 1.0 x 3.8	145.5	0.01/0.05	0.66	0.1	2	1.8
3	0	1	2.00 - 2.00	52.6 x 25.8 x 38.4	109.2	0.49/0.73	0.42	0.05	0.7	1
3	0.089	1.18	2.00 - 2.17	56.2 x 21.7 x 31.1	116.4	0.39/0.55	0.49	0.05	0.9	1.3
3	0.17	1.76	2.00 - 2.73	59.4 x 16.9 x 24.4	122.8	0.28/0.41	0.55	0.07	1.1	1.7
3	0.245	2.72	2.00 - 3.39	62.3 x 11.4 x 16.3	128.6	0.18/0.26	0.61	0.08	1.4	2.1
3	0.3	3.67	2.00 - 3.25	64.3 x 6.8 x 9.2	132.7	0.11/0.14	0.65	0.07	1.6	2.4
4	0	1	2.00 - 2.00	49.2 x 29.2 x 28.9	102.5	0.59/0.59	0.35	0.05	0.5	1
4	0.089	1.19	2.00 - 2.16	52.9 x 25.0 x 25.1	109.8	0.47/0.47	0.44	0.05	0.7	1.5
4	0.17	1.85	2.00 - 2.64	56.2 x 19.9 x 19.8	116.4	0.35/0.35	0.52	0.06	1	2
4	0.245	2.95	2.03 - 2.40	59.1 x 14.2 x 12.7	122.2	0.24/0.22	0.6	0.06	1.3	2.6
4	0.3	4	2.02 - 2.60	61.2 x 9.3 x 6.4	126.4	0.15/0.11	0.67	0.06	1.5	3.1
5	0	1	2.00 - 2.00	47.2 x 31.2 x 22.9	98.5	0.66/0.49	0.31	0.05	0.4	1
5	0.089	1.2	1.99 - 2.18	51.0 x 26.9 x 20.3	105.9	0.53/0.40	0.41	0.05	0.6	1.6
5	0.17	1.95	2.01 - 2.18	54.3 x 21.6 x 15.5	112.6	0.40/0.29	0.51	0.05	0.9	2.3
5	0.245	3.15	2.00 - 2.55	57.2 x 15.6 x 9.0	118.5	0.27/0.16	0.61	0.06	1.2	3.2
5	0.3	4.3	2.00 - 3.19	59.3 x 10.6 x 3.1	122.6	0.18/0.05	0.71	0.07	1.5	3.9
5	0	3.6	7.04 - 7.14	44.6 x 28.6 x 17.8	93.3	0.64/0.40	0.35	0.16	0.3	1
5	0.245	5.65	7.00 - 7.55	54.7 x 13.1 x 4.0	113.5	0.24/0.07	0.72	0.16	1.2	4.3

Table 1 shows values of ε (eccentricity of the noncircular gear) up to 0.3 which was chosen for this table because it is close to a practical limit for most rotors. As ε increases, both the minimum radii of the lobes, *rmin,* and minimum widths of the lobes, *wmin,* decrease and either may limit the acceptable choices for a particular implementation. When *rmin* is too low, the minimum distance to the shaft is too low for the shaft and bearings. When wmin is too low, the lobes are so thin that they may be too weak to withstand the stresses during acceleration and rotation. In some cases, ε may exceed 0.3 but the actual limit depends on manufacturing tolerances, strength of materials, physical constraints for housing size, bearing/shaft clearance, maximum allowed RPM and rotor strength. This family of rotor profiles gives the engineer a family of profiles that can be chosen to fit the application. In general, to maximize airflow, it is best to pick a value of ε as large as possible while satisfying the physical constraints. Note that the airflow loss increases much more slowly than the

net airflow gain as ε increases. In the table, at given RPM, the highest flow is always at the most eccentric profile for the specified number of lobes.

The improved airflow of the new profiles is primarily due to better area efficiency because more of the area, and hence volume, is devoted to air pockets instead of the rotors. A second factor in the improvement with fixed shaft spacing is that the diameter of the lobes is increased which results in a larger housing with more air volume. When comparing two rows with the same number of lobes, the ratio of airflow improvement in the last column is greater than the value obtained by dividing the *Area Efficiencies*. The reason for the greater increase is that for a fixed shaft spacing, the higher ε allows for a larger maximum lobe radius and larger diameter of the housing. Total volume increases as r^2 and this total area increase is multiplied by the *Area Efficiency* increase.

The lambda column shows λ_r, the ratio of minimum to maximum radius of the lobes, along with λ_w, the ratio of the lobe width to the maximum radius..

In Table 1, the *offset* inputs were set to make the minimum gaps a generous 2 mm. This value is intentionally large to show that the losses are still small and that these profiles are good candidates for manufacturing processes with loose tolerances, such as 3D printers.

Table 2 shows the characteristics of rotors with 2-7 lobes, all with the same ε value, but with a much tighter *offset* to make the minimum gaps 0.1mm.

Table 2. Airflow model results for Lobes 2-7 at 1000 RPM with rotor height 100 mm, shaft spacing 80.4 mm, and rotor to housing gap of 0.1 mm. The left three columns are the input values and the other columns are derived by the model. Offsets, gaps, lobes and housing dimensions are all in mm.

Lobes	Gear ε	Offset	Gaps min/avg	Lobes *rmax* x *rmin* x *wmin*	Housing diam	λ_r / λ_w	Area Efficiency	Airflow (m^3/min) loss	net
2	0.245	1.59	0.10 - 1.54	69.7 x 6.3 x 13.8	139.5	0.09/0.20	0.61	0.04	1.8
3	0.245	1.77	0.10 - 1.49	63.2 x 12.4 x 18.2	126.7	0.20/0.29	0.58	0.04	1.4
4	0.245	1.99	0.10 - 0.48	60.1 x 15.1 x 14.6	120.3	0.25/0.24	0.58	0.01	1.3
5	0.245	2.2	0.10 - 0.66	58.2 x 16.6 x 10.9	116.6	0.28/0.19	0.58	0.02	1.2
6	0.245	2.41	0.10 - 0.72	56.9 x 17.4 x 7.7	114.1	0.31/0.14	0.59	0.02	1.2
7	0.245	2.6	0.10 - 0.34	56.0 x 17.9 x 5.2	112.3	0.32/0.09	0.61	0.01	1.2

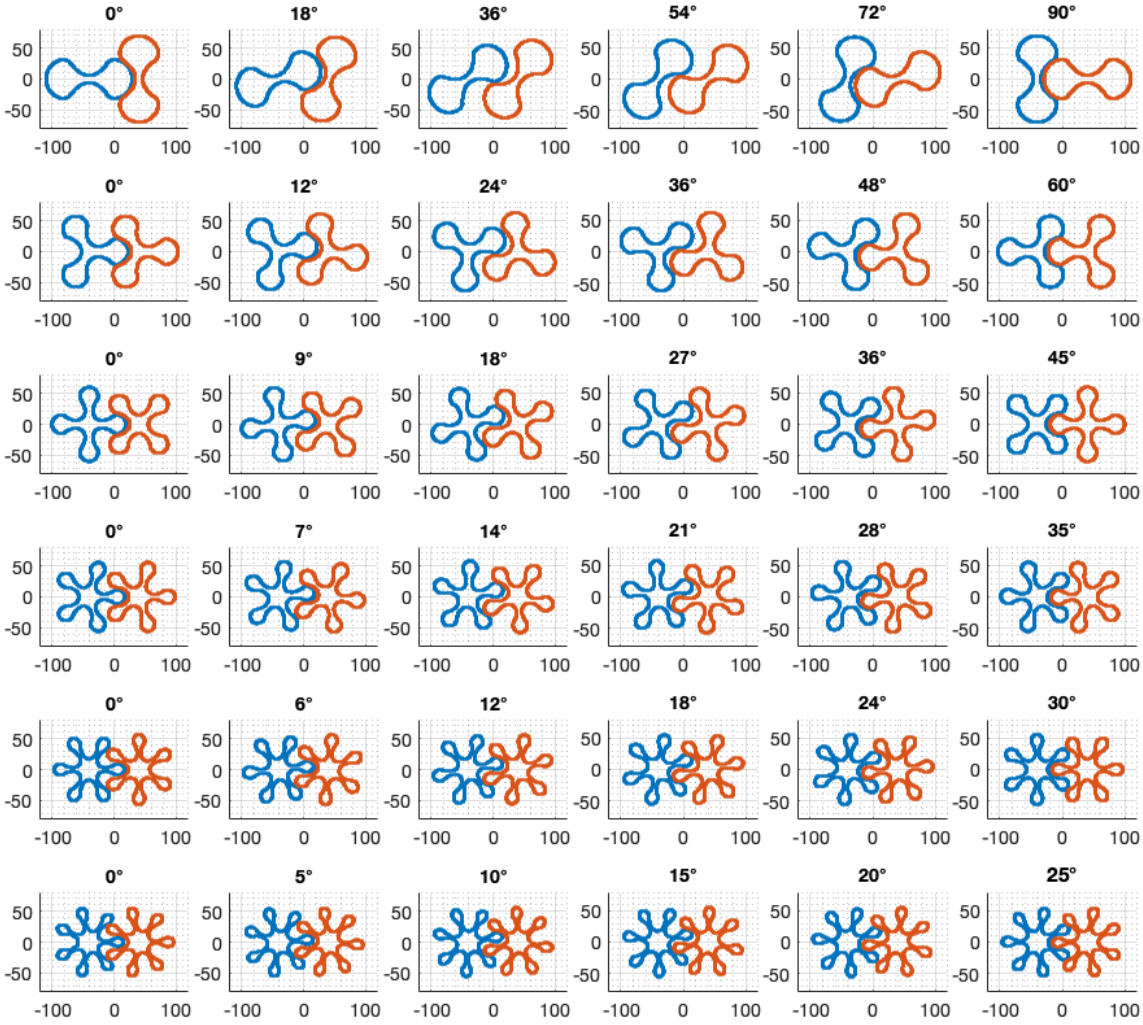

Figure 7. Meshing of rotors with 2-7 lobes with ε = .245 at six different rotations. Minimum gaps are 0.1 mm.

Figure 7 shows each of the six rotors of Table 2 at six different rotation angles. The airflow losses in these cases are due almost entirely to the carryover from the imperfect meshing of the profiles, but the losses are small compared to the large net airflow gained by these highly eccentric profiles. Examining these figures gives visual reinforcement that the carryover volume is small compared to the volume of the air pockets delivered to the discharge port.

Table 3. Airflow model results at 1000 RPM with rotor height 100 mm, fixed housing diameter of 130 mm and rotor-to-housing gap of 2 mm. The left three columns are the input values and the other columns are derived by the model. *Offset* inputs are set to values that make the minimum rotor-rotor gaps close to 2 mm. Offsets, gaps, lobes and shaft spacing dimensions are all in mm.

Lobes	Gear ε	Offset	Gaps min/avg	Lobes *rmax* x *rmin* x *wmin*	Shaft Spacing	Area Efficiency	Airflow (m^3/min) loss	net	ratio
2	0	1	2.00 - 2.00	63 x 20.3 x 58.9	85.3	0.51	0.05	1.22	1
3	0	1	2.00 - 2.00	63 x 31.0 x 46.2	96.0	0.42	0.06	0.98	1
4	0	1	2.00 - 2.00	63 x 37.4 x 37.3	102.4	0.35	0.07	0.81	1
5	0	1	2.00 - 2.00	63 x 41.7 x 31.0	106.7	0.30	0.07	0.69	1
2	0.245	1	1.96 – 3.28	63 x 4.8 x 10.8	73.8	0.63	0.07	1.50	1.22
3	0.245	1	2.02 – 3.42	63 x 11.6 x 16.5	81.3	0.61	0.08	1.43	1.45
4	0.245	1	1.98 - 2.38	63 x 15.2 x 13.7	85.6	0.60	0.06	1.44	1.77
5	0.245	1	2.07 - 2.68	63 x 17.0 x 10.0	88.4	0.61	0.07	1.46	2.12

Table 3 shows a comparison between EH profiles ($\varepsilon = 0$) with highly eccentric profiles ($\varepsilon =$ .245) while holding the housing diameter constant at 130 mm and allowing the shaft spacing to vary. This comparison corresponds to the case when an existing design has a constrained volume for the housing but there is freedom to adjust the shaft spacing and gearing. This comparison shows that the value of the new profiles increases with an increasing number of lobes. With five lobes, the flow is more than double even though the outside dimensions of the housing are unchanged.

4.4. Helical rotors

The Roots profiles described in the equations and figures of this paper apply to either straight-lobe or helical rotors. Helical rotors introduce a twist along the length of the rotor and have been found to have more stable airflow, reduced eddy currents, and increased efficiency [15]. Yao also reported that three-lobe helical rotors have greater airflow, decreased exhaust pressure pulses, and lower noise [16]. Others have investigated rotor profiles for helical Roots blowers [17,18]

The helical twist angle, φ, must not introduce a channel for airflow directly between the input and output ports. When the housing has a semicircular wall for each rotor to contain the air pocket, the total angle of the air pocket (the lobe angle plus the twist angle) must be less than the containment angle of 180°. The air pocket angle is determined by the number of lobes, N, hence

$$\varphi <= \pi/2 - 2\pi/N \tag{7}$$

Table 4. Allowable helical twist angles.

Lobes	Air Pocket angle	Maximum φ	Lobe twists
2	180°	0°	0
3	120°	60°	0.5
4	90°	90°	1
5	72°	108	1.5
6	60°	120°	2
7	51°	129°	2.5

Table 4 shows the maximum allowable twist angle for Roots rotors with 2-7 lobes, although these angles can be increased slightly by extending the housing around each rotor to > 180°. The last column measures the maximum twist angle by the number of lobe twists. A twist of 1 means that the top and bottom of the rotor have the end of the lobe directly above the start of the lobe. When the twist = 1, the airflow should be the same at every rotation angle because every combination of lobe angles is found somewhere between the ends of the rotor. The 3-lobe helical rotors can only be twisted half of one lobe, but those with 4 or more lobes can have a full twist.

If the output port is restricted to less than the full height of the rotor, it is possible to have helical twists greater than that shown in Table 4. The output restriction also causes a compression of the air at discharge which is beneficial in some applications. Zhao has proposed such a structure for an air compressor for a hydrogen fuel cell vehicle [19]. The rotor profiles presented in this paper could also apply to these applications.

4.5. Fabrication

The following technique can be used to fabricate rotors based on equations 4-6: First, a program is written in MATLAB, Python or another language, to implement the equations plus the offsets. The code also exports the X and Y coordinates of the profile into a csv file with sufficient points to produce a smooth curve. In practice, a range from 180 to 1001 points have been used successfully. Next, a 3D CAD program such as Autodesk Fusion uses a script such as ImportSplineCSV to convert the csv file points to a closed spline shape. The shape is then extruded with a twist along the path of a construction line running through the shaft center. The extruded shape is then modified with any other mounting holes or structures, and exported as a STEP file or mesh file. The 3D slicer then imports the STEP or mesh file, slices it, and prints it. Rotors may be 3D-printed with zero infill to make the rotors hollow because hollow rotors are faster to print, consume less material, and avoid uneven fill material which could affect their balance. When the rotors are helical, separate models for left and right twists must be produced and printed.

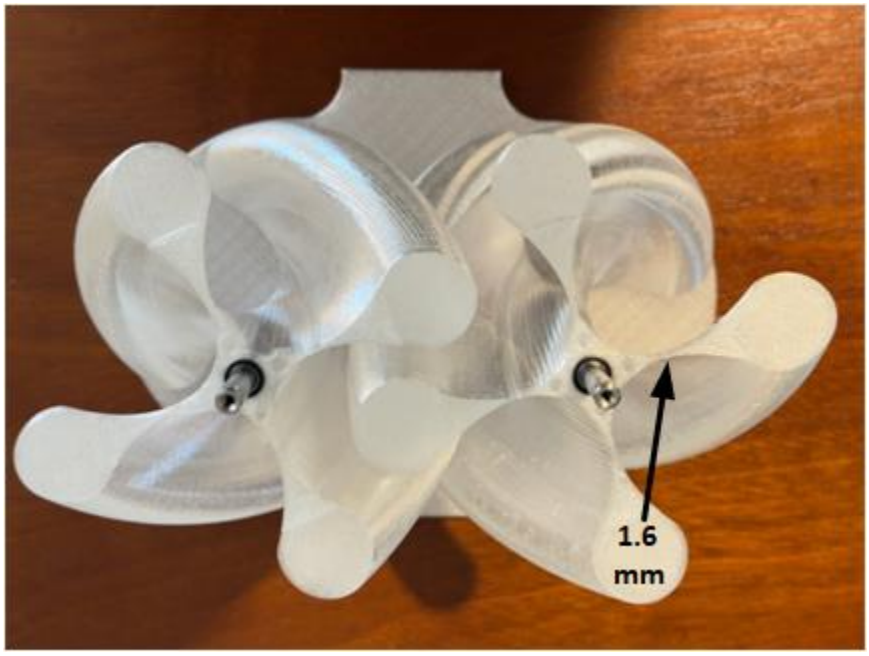

Figure 8. 3D-printed 4-lobe rotors with helix angle 90° and ε = 0.3

Figure 8 shows a 4-lobe helical rotor with a height of 120 mm, minimum gap of 7 mm and a full lobe twist of 90°. For this rotor, the high eccentricity and large minimum gap makes the minimum lobe width just 1.6 mm, as indicated by the arrow. These rotors were printed with the flat lobe ends on the XY bed of the 3d printer to avoid the need for supports and to make the weakest dimension along the axis and not subject to centrifugal forces.

To make a rough estimate of the strength of this rotor, the lobe is held to the shaft by the total cross-section of 1.6 mm times the path length of the lobe height. For a straight-lobe rotor 100 mm high, each lobe would be attached by a cross-section of 160 mm^2. If the lobe is printed with PETG, the tensile strength in the YZ direction is approximately 44 MPa [20] and the force to break off a lobe is 16,000 N. The helical rotor is stronger because the path length of the helix is longer. A more detailed analysis would be required to determine if the strength is sufficient to withstand the stresses encountered from the expected centrifugal forces at maximum rotation rates. If the analysis shows that rotor strength needs to be increased, the family of profiles in this paper makes it easy to do so by making incremental reductions in eccentricity and/or offset. As shown in Figure 6 and Table 1, a small decrease in eccentricity results in a large increase in the lobe width which increases strength at the cost of a small decrease in airflow.

Determining the reliability and strength of the more eccentric profiles is beyond the scope of this paper due to the wide possible choices of materials, dimensions and operational requirements. The strength of the rotors is determined by the rotor material, fabrication methods and rotor dimensions and the expected forces are a function of the maximum motor RPM and the rotor radius. A mechanical engineer designing a Roots blower would define a set of mechanical and operational constraints and then use conventional MCAD tools, such as finite-element analysis, to evaluate the stress and deformation of potential rotors during operation. This paper supplies the key design element missing from standard tools; a way to generate the curves of candidate profiles for the rotors.

4.6. Experimental Verification

Figure 9 shows two sets of rotors that have been 3d-printed in order to verify the airflow modeling results. Both sets have 5 lobes with a helix angle of 72° and are designed for shaft spacing of 80.4 mm and rotor-to-housing gap of 2 mm. The first (purple) set is a traditional EH (epicycloid/hypocycloid) with an eccentricity of 0, meaning that the profile is generated by rolling a circle around another larger circle. The second (blue) set is based on the new profiles using an eccentricity of 0.245. In both cases, the minimum rotor to rotor gap is set at 7 mm. This large gap was required to account for the backlash in the gearing of these prototypes to assure that the rotors do not touch at any angle during the rotation. The last two rows of Table 1 show the inputs and outputs of the MATLAB model for these rotors. The housings have different diameters because, given the same shaft spacing, the eccentric rotor lobes are longer. The rotor to housing gap of 2 mm makes the housing diameters 93.3 and 113.5 mm, respectively.

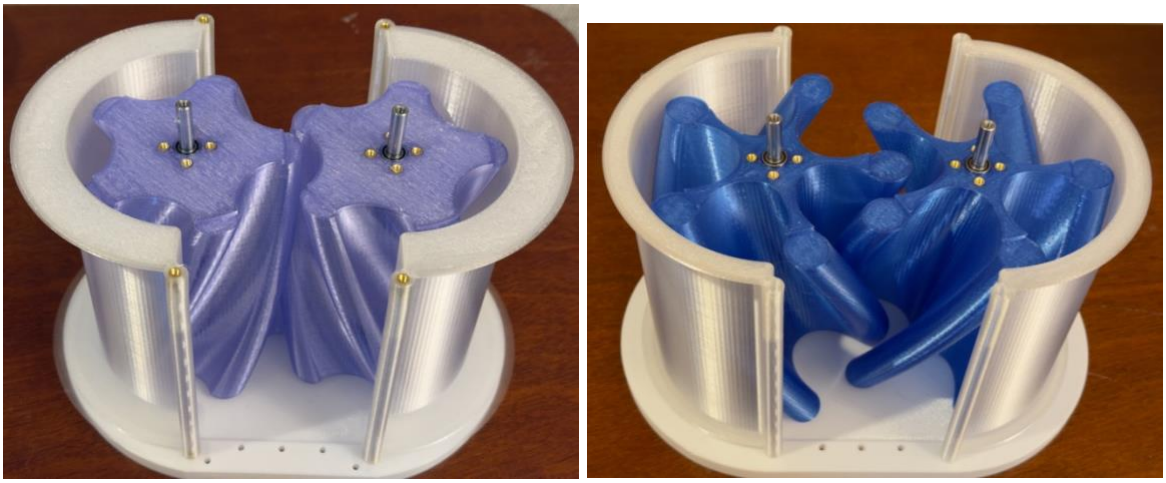

Figure 9. 3D-printed 5-lobe rotors with helix angle 72°. Left $\varepsilon = 0$, right $\varepsilon = 0.245$

Figure 10 shows the test setup. The blower assembly has 3d-printed plates for attaching the shafts, the electronics and the brushless DC motor/gearing to drive the rotors. The same assembly was used to test both sets of rotors. After the EH rotors were tested, the rotors and housing shells were removed and replaced with the eccentric rotors along with their larger diameter shells. The same assembly was used to avoid differences that could have otherwise been introduced.

The suction port in back is kept completely open as shown in Figure 9. The discharge port in front has a plate that reduces the output flow to a 51mm diameter circle which is attached to a flow straightener that is 60 mm long with 6 mm diameter hexagonal partitions. The area of the suction and discharge ports are identical for both rotor enclosures. A Bonvoisin Hot Wire Anemometer (Model Roy-9) measures the airflow. A bracket holds the inlet of the anemometer in the center of the output airflow 12mm from the exit of the flow straightener.

Figure 10. Experimental setup.

The motor controller is a custom design using a TI DRV8308 motor controller and STM32L072 processor with code written in C. Hall effect sensors communicate the rotor position to the motor controller, and the processor uses the hall effect signals to determine and display the motor RPM.

The code controlling the motor was modified to remove the closed-loop speed control and instead to allow the selection of the PWM (pulse-width modulation) duty cycle 10, 25 or 100%. The motor speed is then easily adjusted by selecting a PWM level and adjusting the voltage from the power supply (FNIRSI IPS3608). The motor controller accepts 10-30 V input and the speed scales in proportion to the voltage times the PWM. Maximum speed is limited to just over 3000 RPM.

Measurements were performed under laboratory ambient conditions, with air temperature in the range 21.8–22.4 °C and atmospheric pressure (approximately 1 atm). Thermodynamic properties used in the analysis were evaluated at these conditions, and the working fluid was modeled as an ideal gas. Table 5 shows the raw data from the measurements.

Table 5. Blower measurements of 3d-printed rotors with ε = 0 (purple) and ε = 0.245 (blue)

airflow m/s	RPM		PWM		Voltage (V)		Power (W)		Sound (db)	
	ε 0	ε 0.245	ε 0	ε 0.245	ε 0	ε 0.245	ε 0	ε 0.245	ε 0	ε 0.245
1	680	180	10%	10%	20.5	21.6	2.2	2.5	49	45
2	1600	400	25%	25%	16.2	11.3	5.2	3.1	62	49
3	2460	640	100%	25%	13	17.3	9.9	6.8	70	54
4	3000	880	100%	100%	17.3	12.6	17.6	12.4	74	58

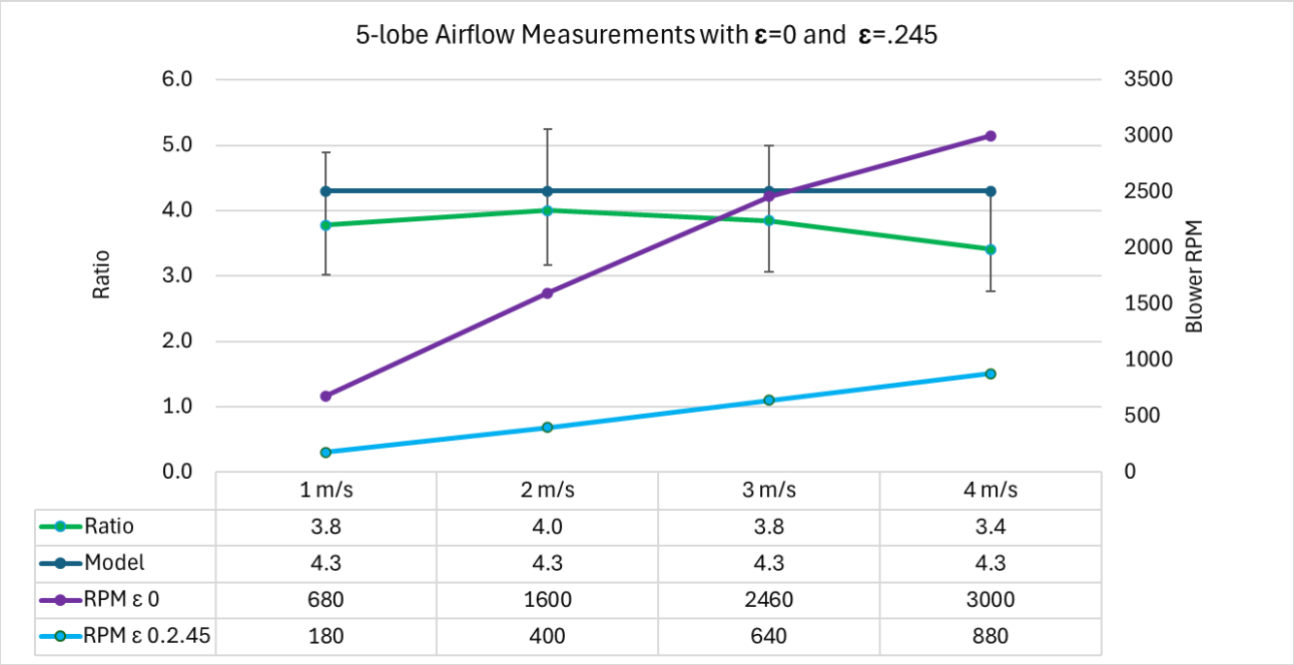

	1 m/s	2 m/s	3 m/s	4 m/s
Ratio	3.8	4.0	3.8	3.4
Model	4.3	4.3	4.3	4.3
RPM ε 0	680	1600	2460	3000
RPM ε 0.2.45	180	400	640	880

Figure 11. Experimental verification of airflow improvement with eccentric lobes. At a fixed airflow velocity, measurements show that the EH rotor requires the motor to run 3.4 to 4 times faster than the eccentric rotor. The airflow model in Table 1 shows a 4.3 times factor in airflow, and this falls within the +- 5% error bars shown on the graph.

The measurements were performed at four different airflow velocities attainable by both rotors. Voltage was adjusted in small steps until the anemometer reading centered on the desired velocity. Each measurement was repeated at least 3 times and the readings were repeatable within 5% which is shown by error bars in the graph. Relative measurements of the two rotors was used for verification because absolute airflow cannot be easily determined. The airflow in Table 1 assumes zero backpressure, while the smaller output port makes the internal pressure higher than ambient. By comparing two rotors producing the same output velocity, any backpressure reduces the velocity of both rotors in the same way.

Other data from Table 5 shows that for higher air flows, the slower speed contributed to lower power and quieter operation. The numbers shown in the raw data are strongly affected by the type of motor, gearing, bearings and tolerances and cannot be directly compared to other implementations, but running the motor slower for the same airflow should always be somewhat quieter. The magnitude of the sound reduction would be affected by many factors such as sound insulation, gearing and bearings,

Another improvement of the eccentric rotors is weight reduction. The 3d-fabricated rotors are hollow, but in most applications, rotors would be cast or machined from aluminum or steel. The Autocad Fusion program used to generate the rotor profiles was used to assign materials to solid rotors, then calculate the weights. With steel rotors, each EH rotor is 3.8 kg compared to 2.5 kg for the eccentric rotor. With aluminum, each EH rotor is 1.3 kg compared to .47 kg. In some applications, this 36% weight reduction could be significant.

4.7. Comparison with other profiles

It can be difficult to compare Roots profiles presented in different papers because they present results in different ways. Some papers omit area efficiency calculations, and many do not specify rotor dimensions. However, many papers include enough information to determine the ratio of the minimum to maximum diameter of the lobes, as shown in Table 6.

Some papers give this ratio (or its inverse) directly, some give the rotor dimensions, and some give the shaft spacing and chamber radius (~= maximum rotor radius) which allows derivation of the minimum radius. Half of the shaft spacing is the pitch radius. Subtracting pitch radius from the chamber radius gives the delta to be added or subtracted from the pitch radius to determine the maximum and minimum rotor radii.

Table 6. Comparison of length ratios of lobes from recent papers on improved Roots profiles.

Reference	Rotor type	Lobes	SS	Lobe rmax	Lobe rmin	λ_r
Shujun 2011 [21]	Traditional involute	3				0.683
	Improved involute	3				0.680
Wu 2018 [3]	IVEC (Involute and Variable-Extended Cycloids)	2	80	63	17	0.270
		3	66	44	22	0.500
Xing 2021 [22]	Four curves plus involute	3	280	209.75	70.25	0.335
		6	280	185	95	0.514
Zhao 2022 [19]	Helical 160 deg wrap	4	43.36	32.05	11.31	0.353
Zhou 2023 [23]	Four arcs, epicycloid, and involute	3				0.680

The last column shows λ_r, the ratio of minimum to maximum radius of the rotor. Smaller numbers indicate lobes that are more eccentric and that devote more area to air pockets instead of the rotor itself. The smallest number from these recent papers is 0.270, meaning that the lobe length is 3.7 times its width. Comparing these values with those from Tables 1 and 2, the new profiles clearly have much larger areas devoted to air pockets and hence will have greater air flow. In Table 1, with $\varepsilon = 0.3$, λ_r ranges from .01 to .18, indicating length-to-width ratios of 5.6:1 to 100:1. Figure 10 below, from one of the references, shows rotor profiles that clearly have smaller air pockets than the new profiles shown in Figure 6.

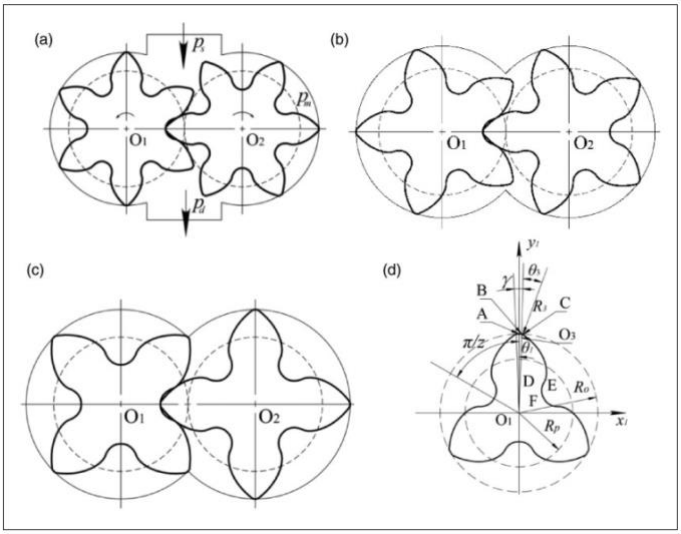

Figure 8. Prior Roots profiles from Figure 5 of Xing 2021 [22].

5. MATLAB code

MATLAB code for creating and modeling the new profiles is publicly available in a GitHub repository [25]. The code has an interactive mode that allows setting the input parameters and

viewing plots of pairs of the generated profiles at six different rotation angles. Each profile also produces outputs including rotor dimensions and modeled flow estimates. Inputs can be made either assuming fixed shaft spacing or fixed housing diameter. The modeled profile can optionally generate a CSV file of the generated spline. The CSV file is of the form readable by Autodesk Fusion and could be modified for other 3D CAD programs used for fabrication.

The MATLAB code also has a batch mode for generating groups of profiles to make it easier to compare options and create tables similar to those in this paper.

6. Limitations

The analysis of flow in Tables 1-3 are based on simplifying assumptions for airflow. They are based on a simple model that assumes backflow due to gaps between the rotors, but the analysis does not include detailed modeling of turbulence or pulsations. Future work could include computational fluid dynamics (CFD) analysis of some selected groups of rotor profiles. The models include no analysis of boundary conditions for input and output and do not examine different input and output throat lengths or airflow restrictions. The effect of temperature changes from input to output are not included. No adjustments to airflow have been made for leakage at the ends of the rotors or at the rotor to shell gaps. The same limitations have been made for all rotor profiles, including the profiles used as the basis for comparison.

The family of profiles in this paper is based on input parameters that can be varied up to and beyond the point that a profile is no longer viable. Both high eccentricity and large offsets can make the curves defining the sides of a lobe intersect or reach the point where the lobe is too thin to stand up to the centrifugal forces of rotation. In other cases, the diameter of the center may too small for the required shaft and bearings. The point where the rotor profile is no longer feasible is a function of a particular mechanical design based on the materials used, size of the rotor, maximum RPM, bearing choices and machining tolerances. The MATLAB code does not restrict the design space but presents the minimum rotor dimensions to help a designer adjust the input parameters to stay within the design margin of any particular design.

The experimental verification was done only on one set of eccentric and standard EH 5-lobe helical rotors. The measurements did not attempt to measure internal or external pressures, but all comparisons were made with the same motors and input and output ports at the same measured airflow. Turbulence and pulsation were not modeled or measured,

7. Conclusions

This paper has described and analyzed a new family of high-flow Roots profiles. The simplified equations and public GitHub code give engineers new tools for designing a range of Roots profiles that are more easily implemented than those based on more complex mathematical derivations. The equations simply describe new profiles based on a circle rolling around a noncircular gear, and the simplifications stem from the lessons learned in the analysis of the coin rotation paradox. The derivation extends previous work in noncircular gear theory with equations that define a new family of identical multi-lobe circular gear profiles. Circles are rolled around the noncircular gears to produce profiles that are more eccentric and higher-flow than traditional Roots profiles. Interference between rotors in the resulting profiles is eliminated by offsetting the profiles. Estimates of the flow rates show that the small amount of carryover (reverse flow) is more than overcome by the greater

flow rates of the new profiles. The profiles can be built as either straight-lobe or helical rotors. The new profiles also provide reduction of the weight of the rotors.

The airflow increase predicted by the model has been validated by constructing and comparing blowers with traditional and eccentric 5-lobe helical rotors. Testing showed that the new profiles can produce the same airflow at much lower RPM. The slower operation also showed improvements in acoustic noise and power requirements.

Roots blowers with relaxed manufacturing tolerances, high air movement, and low noise may see more applications in home devices currently served by squirrel cage blowers or ducted fans. New applications may include air filters, range hoods, bathroom vents, hair dryers, and leaf blowers. The profiles described in this paper may be a step toward these wider applications.

Acknowledgments

The author thanks Doug Jewett, Chuck McManis, Joseph N. West, Philip Rakity, and Simon Quellen Field for helpful technical discussions and assistance in preparing this document.

Data Availability Statement

The simulated data used to support the findings of this study are included within the article and the publicly available MATLAB code.

Disclosure

A preprint has previously been published [24].

Conflicts of Interest

The author declares no conflicts of interest. All funding for this project was provided by the author.

Funding

No funding was received for this manuscript.

References

1. P.H Roots, "Rotary blower," U.S. Patent 2369 (1860).
2. W.L. Palmer and I.W. Knox, "Improvement in rotary pressure-blowers, " U.S. Patent 166,296, (1875).
3. Wu, Yu-Ren, and Van-The Tran. "Generation method for a novel Roots rotor profile to improve performance of dry multi-stage vacuum pumps." *Mechanism and Machine Theory* 128 (2018): 475-491.
4. Ucer, S., and I. Celik. "Analysis of flow through roots blower systems." (1980).

5. Zhou, Shuangmei, et al. "The effects of design parameters on performance of a novel roots profile." *International Journal of Hydrogen Energy* 48.6 (2023): 2368-2384.
6. Tien, Tran Ngoc, and Nguyen Hong Thai. "A novel design of the roots blower." *Vietnam Journal of Science and Technology* 57.2 (2019): 249-260.
7. Tong, Shih-Hsi, and Daniel CH Yang. "Generation of identical noncircular pitch curves." (1998): 337-341.
8. Litvin, Faydor L., et al. "Design and investigation of gear drives with non-circular gears applied for speed variation and generation of functions." *Computer methods in applied mechanics and engineering* 197.45-48 (2008): 3783-3802.
9. Bair, Biing-Wen, et al. "Tooth profile generation and analysis of oval gears with circular-arc teeth." *Mechanism and machine theory* 44.6 (2009): 1306-1317.
10. Tong, Shih-Hsi, and Daniel CH Yang. "Generation of identical noncircular pitch curves." (1998): 337-341.
11. Tien, Tran Ngoc, and Nguyen Hong Thai. "A novel design of the roots blower." *Vietnam Journal of Science and Technology* 57.2 (2019): 249-260.
12. Zarębski, Igor, and Tadeusz Sałaciński. "Designing of non-circular gears." *Archive of Mechanical Engineering* (2008): 275-292.
13. Harris, Michael J. "The SAT Problem That Everybody Got Wrong." *Scientific American*, 20 June 2023.
14. Ucer, S., and I. Celik. "Analysis of flow through roots blower systems." (1980).
15. Tran, Ngoc-Tien, and Duc-Minh Nguyen. "Analysis of flow characteristics of cylindrical and helical type multi-lobe roots blower." *EUREKA: Physics and Engineering* 1 (2023): 67-75.
16. Yao, Ligang, et al. "Geometric analysis and tooth profiling of a three-lobe helical rotor of the Roots blower." *Journal of Materials Processing Technology* 170.1-2 (2005): 259-267.
17. Xing, Linfen, et al. "Analysis and development of a roots-type air compressor with fixed internal compression for fuel cell system." *Proceedings of the Institution of Mechanical Engineers, Part A: Journal of Power and Energy* 236.1 (2022): 51-60.
18. Li Tran, Ngoc-Tien, and Duc-Minh Nguyen. "Analysis of flow characteristics of cylindrical and helical type multi-lobe roots blower." *EUREKA: Physics and Engineering* 1 (2023): 67-75., Dantong, et al. "Development and analysis of novel six-lobe helical rotors for hydrogen fuel cell vehicle roots blowers." *International Journal of Hydrogen Energy* 46.59 (2021): 30479-30493.
19. Zhao, Bin, et al. "Investigation of 3D transient flow and discharge pressure pulsation of helical roots air compressor for hydrogen fuel cell vehicle." *Proceedings of the Institution of Mechanical Engineers, Part C: Journal of Mechanical Engineering Science* 236.23 (2022): 11231-11239.
20. Ultimaker PETG Technical Datasheet, https://um-support-files.ultimaker.com/materials/2.85mm/tds/PETG/Ultimaker-PETG-TDS-v1.00.pdf
21. Shujun, Wang, et al. "The improvement study of involutes profile type rotor profile in Roots vacuum pump." 2011 International Conference on New Technology of Agricultural. IEEE, 2011.
22. Xing, Linfen, et al. "Performance improvement of a large capacity Roots blower based on profile modification." *Proceedings of the Institution of Mechanical Engineers, Part C: Journal of Mechanical Engineering Science* 235.13 (2021): 2386-2394.
23. Zhou, Shuangmei, et al. "The effects of design parameters on performance of a novel roots profile." *International Journal of Hydrogen Energy* 48.6 (2023): 2368-2384.
24. Horst, Robert. "A family of high-flow Roots blower profiles based on non-circular gears and the coin rotation paradox." engrXiv, https://doi.org/10.31224/4850 (2025).
25. Horst, Robert, *RootsProfileDesigner,* MATLAB code, Version 0.2.0, GitHub, 19 Apr. 2026, https://github.com/RobertHorst/RootsDesigner